



Ce-doped LiF–SrF₂ eutectic scintillators for thermal neutron detection produced at different solidification rates

Takayuki Yanagida^{a,*}, Yutaka Fujimoto^b, Kentaro Fukuda^c, Noriaki Kawaguchi^c, Kenichi Watanabe^d, Atsushi Yamazaki^d, Akira Uritani^d, Valery Chani^b

^a Kyushu Institute of Technology, 2-4 Hibikino, Wakamatsu-ku, Kitakyushu 808-0196, Japan

^b Institute for Materials Research, Tohoku University, 2-1-1 Katahira, Aoba-ku, Sendai 980-8577, Japan

^c Tokuyama Corporation, 1-1 Mikage-cho, Shunan-shi, Yamaguchi 745-8648, Japan

^d Quantum Science and Energy Engineering, Graduate School of Engineering, Nagoya University, Furo-cho, Chikusa-ku, Nagoya 464-8603, Japan

ARTICLE INFO

Article history:

Received 28 November 2012

Received in revised form 25 February 2013

Accepted 28 February 2013

Available online 21 March 2013

Keywords:

Eutectic scintillators

LiF and SrF₂ layers

Ce³⁺ doping

Neutron detection

ABSTRACT

Ce 0.1% doped LiF–SrF₂ eutectic scintillators were produced by vertical Bridgman method at various solidification rates of 1, 5, 20, 80, 320, and 1280 mm/hr. The LiF contained 95% of ⁶Li. The SEM images of the samples solidified at 1–80 mm/hr demonstrated clear lamellar structures. The α -ray induced radio-luminescence spectra of the scintillators had intense emission peak at 310 and 330 nm due to the emission from Ce³⁺ 5d–4f transition of Ce:SrF₂ layers. When the samples were irradiated with ²⁵²Cf neutrons, they exhibited almost the same light yields of 4500–5500 ph/n and typical decay times of 120–160 ns. The optimal layer thickness of LiF–SrF₂ was determined to be 0.9 μ m.

© 2013 Elsevier B.V. All rights reserved.

1. Introduction

Scintillation detectors, which convert energy of a single photon (X- and γ -ray) or other high-energy particles into hundreds of visible–ultraviolet photons, have been playing a major role in many fields of radiation detection, including medical imaging [1], security [2], astrophysics [3], particle physics [4] and well logging [5]. Compared with semiconductor based radiation detectors [6,7], they are easy to handle, and they have greater detection efficiency. Regarding these applications, scintillators for thermal neutron detection have recently attracted much attention because of deficit of ³He gas [8,9]. Up to now, most of the thermal neutron detectors were gas proportional counters filled with ³He gas, because ³He has high thermal neutron cross section and low background γ -ray sensitivity [10]. However, current demand for ³He gas highly exceeds its supply because tritium is no longer generated in nuclear experiments except nuclear reactors during weapon production. The natural abundance of ³He is approximately 10^{−6} only, and it can be generated by the decay of tritium. The huge disproportion between the demand and the supply of the ³He gas highly motivates academia and industry to develop novel inorganic scintillators suitable for the thermal neutron detectors to replace existing ³He based systems.

One of the candidates for such application is ⁶Li containing material, because ⁶Li has a high probability (940 barn at 25 meV) of interaction with neutrons based on ⁶Li(n, α)³H reaction with high Q-value of 4.8 MeV. Recently, ⁶Li based scintillators, including Ce³⁺ and Eu²⁺ doped ⁶LiCaAlF₆ were developed, and they demonstrated acceptable scintillation responses under ²⁵²Cf neutron irradiation [11–18]. In addition to LiCaAlF₆ scintillators, ⁶Li-based eutectics are now considered as appropriate materials for radiation detectors. LiF-containing eutectics are examples of such materials, and LiF/CaF₂ eutectic composite doped with Mn was first proposed for dosimeter applications [19]. It was recently studied as a neutron scintillator when doped with Eu²⁺ [20]. Following these reports, evaluation of the neutron responses of ⁶LiF/CaF₂:Eu [21] and ⁶LiF–SrF₂:Eu [22] with different Eu concentrations was also performed. In the eutectic scintillators, the neutrons first interact with the ⁶LiF layer that is approximately 1–10 μ m thick. After the nuclear reaction, the generated charged particles excite CaF₂ or SrF₂ (scintillator) layers. Ideally, after all the energy is deposited by the CaF₂ or SrF₂ layers, this energy is converted to scintillation photons. It is well known that Eu²⁺ [23–27] or Ce³⁺ [28–30] doped CaF₂ or SrF₂ exhibit excellent scintillation properties. Therefore, these substances are well suitable as scintillator layers. The LiF–SrF₂ system is especially promising, because molar ratio at the eutectic composition is 81.5:18.5 [31] that results nearly identical volumetric fraction of 56:44. Thus, well-aligned lamellar structure can be easily produced, and this contributes to relatively homogeneous

* Corresponding author. Tel.: +81 93 695 6049; fax: +81 93 695 6049.

E-mail address: yanagida@lisse.kyutech.ac.jp (T. Yanagida).

energy deposition from charged particles. Another advantage of CaF_2 and/or SrF_2 is their low density. This reduces sensitivity of the scintillators to background gamma-rays. In addition, high efficiency of the neutron detection is realized due to high Li content in the $\text{LiF-CaF}_2/\text{SrF}_2$ eutectics. Therefore, compared to conventional neutron scintillators, such as Li-glass (e.g., [32]), Eu:LiI (e.g., [33]), and LiF-ZnS (e.g., [34]), the thermal neutron cross sections of the above eutectics is 50% higher than those of conventional materials with the same sample thickness (see Fig. 1 in [21]).

In the present report, the Ce^{3+} 0.1% activated LiF-SrF_2 eutectic scintillators produced at different solidification rates are discussed. The main goal of this project was to evaluate the optimum thickness of the LiF and SrF_2 layers experimentally because the output scintillation intensity is a function of the attenuation of the charged particles in the LiF layer and deposited energy in the Ce:SrF_2 (scintillator) layer. To our knowledge, this is a first report about Ce^{3+} doped eutectic scintillators. It is generally impossible to predict actual output of scintillation photons. Therefore, experimental examinations were necessary to determine the optimum layer thickness that depends on the solidification rate. For all the samples, scanning electron microscope (SEM) images, α -ray induced radioluminescence, and ^{252}Cf induced pulse height spectra were systematically studied to evaluate their physical performance including light yield and decay time profiles.

2. Experimental

2.1. Sample preparation

High-purity (99.99%) fluoride powders of LiF , SrF_2 , and CeF_3 (Stella Chemifa Corporation) were used as starting materials. The LiF and SrF_2 powders were mixed in 80:20 ratio that correspond to the eutectic composition. The CeF_3 was added in amount of 0.1 mol% with respect to SrF_2 . The ^6Li -enriched (95%) LiF was used to achieve high neutron detection efficiency. The mixtures were placed into graphite crucibles, and the Bridgman method was used to produce $\text{LiF-SrF}_2\text{:Ce}$ eutectics with ordered lamellar structure. In the unidirectional solidification processes such as Bridgman, Czochralski, or micro-pulling-down method, LiF and SrF_2 phases deposit from the melt on their own forming solid phases. Thus, each phase grows along the solidification direction. As a result, the as-produced solids often demonstrate geometrically ordered structure.

For the eutectics growth, the preheating treatment of the starting materials was performed under vacuum to eliminate water and oxygen traces. Subsequently, high-purity Ar gas was introduced into the growth chamber. Subsequently, the mixture of the starting materials was melted at 1100 K. Thereafter, the unidirectional solidification process was started, and it was controlled by speed of displacement of the crucible in downward direction to the bottom part of the chamber where the temperature was maintained to be below the melting point of the eutectic, 1044 K [31]. The as-produced bulk eutectic ingots were cut into wafers perpendicular to the solidification direction and optically polished to be suitable for inspection of their scintillating performance. In order to evaluate typical thickness of the LiF and Ce:SrF_2 layers, SEM back scattered electron (BSE) images were taken.

2.2. Characterization methods

In practice, the scintillators are excited by the neutron irradiation with charged particles produced from the $^6\text{Li}(n,\alpha)^3\text{H}$ nuclear reaction. To simulate this process in laboratory conditions, the ^{241}Am 5.5 MeV α -ray induced radioluminescence spectra were recorded using JASCO FP8600 fluorescence spectrometer at room

temperature. The main purpose of the radioluminescence measurements was to detect emission wavelength under α -ray excitation. This was necessary to select adequate photodetector for the pulse height examination. Because the emission intensity of this kind of integrated type measurement is not a quantitative value, we cannot discuss the light yield of scintillators by radioluminescence intensities except the comparison of samples with the same size and similar chemical composition (similar stopping power) under the same geometry. The detailed description and geometry of the α -ray induced radioluminescence measurements was reported previously [35].

In the pulse height measurements, the eutectic samples were wrapped with several layers of Teflon tape to collect scintillation photons. The samples were then coupled to an ultra bi-alkali photomultiplier tube (PMT) R7600-200 (Hamamatsu) with optical grease (OKEN 6262A). The high voltage of -700 V was supplied (ORTEC 556), and the signals were read out from the anode of the PMT. The neutron source of ^{252}Cf was enclosed in a polyethylene container of 43 mm thickness for thermalization of fast neutrons. In order to cut the background γ -rays, the samples were surrounded by 5 cm thick Pb blocks. Once a neutron from the ^{252}Cf was detected, the signals were fed into the pre-amplifier (ORTEC 113) and then to the shaping amplifier (ORTEC 572) with 2 μs shaping time. After converting to digital signals by a multi channel analyzer (Amptek, Pocket MCA 8000A), they were recorded to a computer. To evaluate the absolute light yield, Li glass scintillator GS20 (6000 ph/n [36]) was used as a standard. The quantum efficiencies at 330 nm (emission wavelength of Ce:LiF-SrF_2) and 395 nm (emission wavelength of Li-glass) were almost the same ($\sim 40\%$). By using the same setup, the samples were irradiated using ^{137}Cs and ^{57}Co sources to grasp γ -ray induced light yield. At the same time, decay time profiles were recorded by WE7311 digital oscilloscope (Yokogawa). The obtained decay time profiles were averaged over 100 times.

3. Results and discussions

3.1. SEM analysis

The cut and polished Ce doped LiF-SrF_2 eutectic specimens had typical dimensions of $\varnothing 12 \text{ mm} \times 1 \text{ mm}$. Fig. 1 illustrates view of the specimens ready for the characterizations. The samples produced at greater solidification rates were not sufficiently transparent due to low uniformity of the lamellar structure. To observe details of the lamellar structure, the microscopic images were taken using SEM. Fig. 2 demonstrates such images made for the samples produced at different solidification rates. Bright fractions of the images represent substances containing heavier elements. This way, the black and gray colored phases correspond to the LiF and SrF_2 , respectively.

It is expected that Ce^{3+} was mostly incorporated into SrF_2 structure (phase) because the ionic radius of Ce^{3+} (1.14 Å) is closer to that of Sr^{2+} ion (1.26 Å) when compared to that of Li^+ (0.92 Å). Moreover, the charge of the Ce^{3+} guest (dopant) ion is +3 that is closer to that of Sr^{2+} host ion (+2) when compared to that of Li^+ (+1). Thus, integration of the Ce^{3+} into the SrF_2 structure creates less stresses and fewer structural defects (vacancies and/or interstitials) when compared with integration of the Ce^{3+} into the LiF . Both these factors make incorporation of the Ce^{3+} into the SrF_2 preferable.

LiF and Ce:SrF_2 phases were clearly separated in the all SEM images. No impurity phases, such as agglomerations of CeF_3 , were detected in the images. The solids produced at solidification rates of 1–80 mm/hr had well ordered lamellar structures. However, those produced at 320–1280 mm/hr were not uniform with considerable amount of grains present. Fig. 3 illustrates the relation

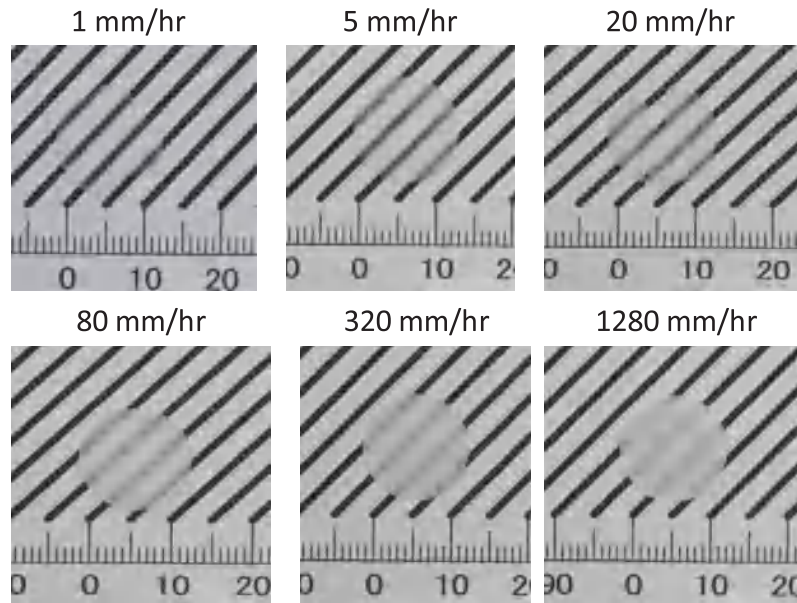


Fig. 1. View of Ce 0.1% doped LiF–SrF₂ eutectic scintillators produced at different solidification rates.

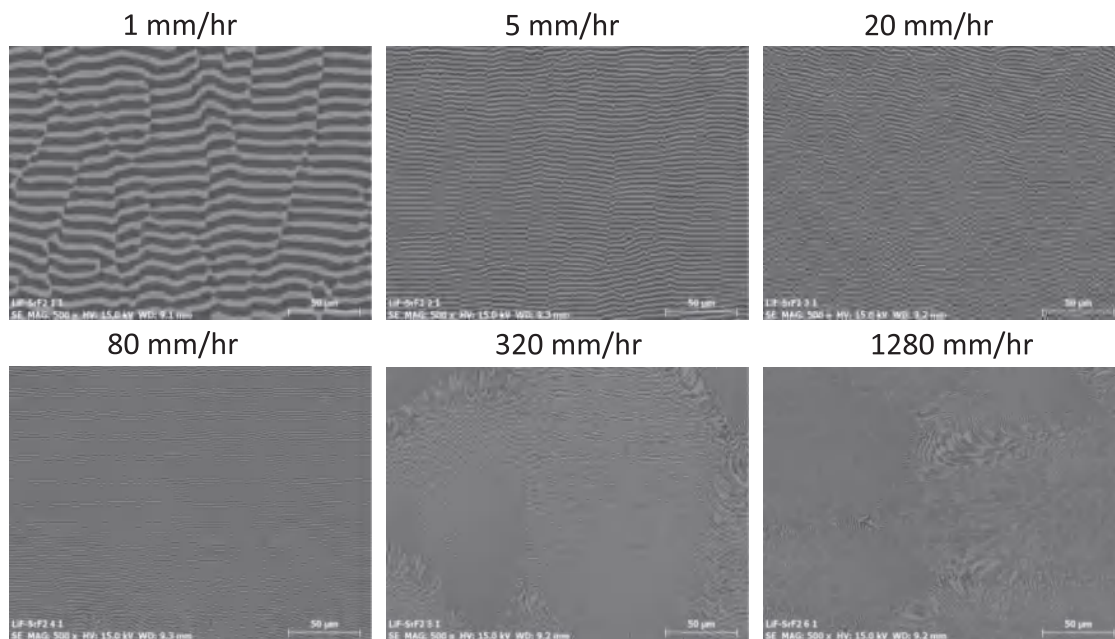


Fig. 2. SEM images of eutectic scintillators produced at different solidification rates.

between the solidification rate and the layer thickness. As it was expected, the layer thickness decreases monotonically with increase of the solidification rate. Typical thicknesses of the LiF–SrF₂ layers were 5, 2, 1.5, and 0.9 μm for the eutectics solidified at 1, 5, 20, and 80 mm/hr rates, respectively.

3.2. Scintillation properties of Ce-doped LiF–SrF₂ eutectic

Radioluminescence spectra are demonstrated in Fig. 4. Broad and intense emission peaks were detected at 310 and 330 nm wavelengths as a result of Ce³⁺ 5d–4f transitions. In all the samples, broad emission peak was observed at 270 nm. This peak could be attributed to the self-trapped exciton (STE) luminescence, which was reported for pure SrF₂ scintillator [37,38]. A broad peak discovered at 370 nm for the thinner layered sample (1 mm/hr) is also

typical for the STE emission because the same peak was detected for pure SrF₂ examined under X-ray excitation [36]. As for the radioluminescence measurements, the 1.5 μm layered sample demonstrated the highest emission intensity. Thus, it was confirmed that the LiF–SrF₂:Ce eutectic solids act as a scintillator excited by charged particles.

Fig. 5a illustrates pulse height spectra of the LiF–SrF₂:Ce eutectic scintillators recorded under ²⁵²Cf neutron irradiation and compared with that of conventional neutron scintillator, Li-glass GS20 [32]. The thermal neutron peaks were clearly detected in all the samples. The quantum efficiencies at emission peaks of Li-glass and Ce:LiF–SrF₂ were similar (approximately 40%), and it was possible to compare their light yield directly based on ²⁵²Cf neutron peak positions. Among the discussed eutectic samples with different layer thicknesses, 0.9 μm layered one demonstrated the highest light yield

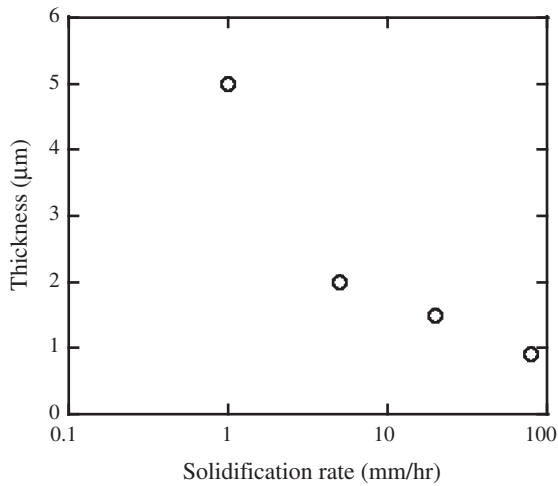


Fig. 3. Typical layer thickness vs. solidification rate.

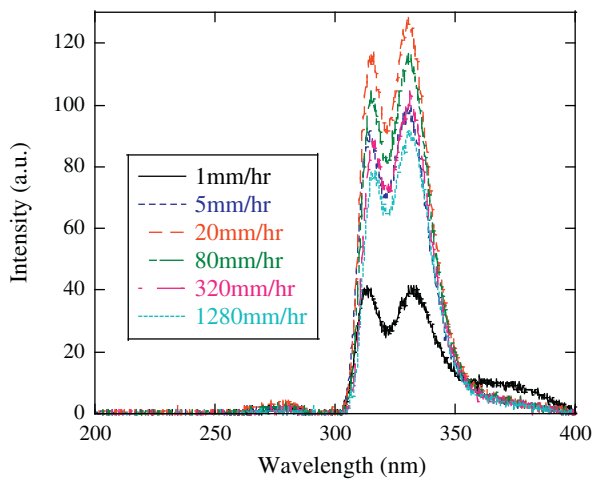


Fig. 4. Radioluminescence spectra of Ce 0.1% doped LiF-SrF₂ observed under α -particle irradiation from ²⁴¹Am source ~5.5 MeV energy.

of 5500 ± 500 ph/n. Then, Fig. 5b compares ¹³⁷Cs and ¹²²Co γ -ray induced pulse height spectra of the 80 mm/hr sample with that of induced by neutrons. Based on the Compton-edge (480 keV) of ¹³⁷Cs at ~150 ch and photoabsorption peak (122 keV) of ⁵⁷Co, the γ -ray induced light yield resulted 2600–2800 ph/MeV. Thus, $\alpha\beta$ ratio of this material was evaluated to be approximately 0.4.

Fig. 6 presents neutron induced light yields as a function of the solidification rate. Thus, the most favorable solidification rate (layer thickness) from the point of view of scintillation light yield was well determined in the materials reported here. As the layers became thinner, the light yield increased because the energy loss of the charged particles in the LiF layer decreased. The observed light yield was similar to that of Eu:LiF-SrF₂ system [22] but lower than that of Ce:SrF₂ [37] possibly due to opacity of the eutectic samples. Low light yield of the samples produced at 320 and 1280 mm/hr solidification rates is attributed to the non-uniformity of the lamellar structures and Ce concentration discussed later.

Fig. 7 shows the decay lifetime profile of the sample produced at 80 mm/hr rate. In all eutectics, decay lifetime profiles were well reproduced by the double exponential function. The main decay lifetime components of this 80 mm/hr sample were 137 ns and 732 ns. The decay time constants of the LiF-SrF₂:Ce eutectic scintillators are plotted as a function of the solidification rate in Fig. 8. The faster component was around 120–160 ns, and the

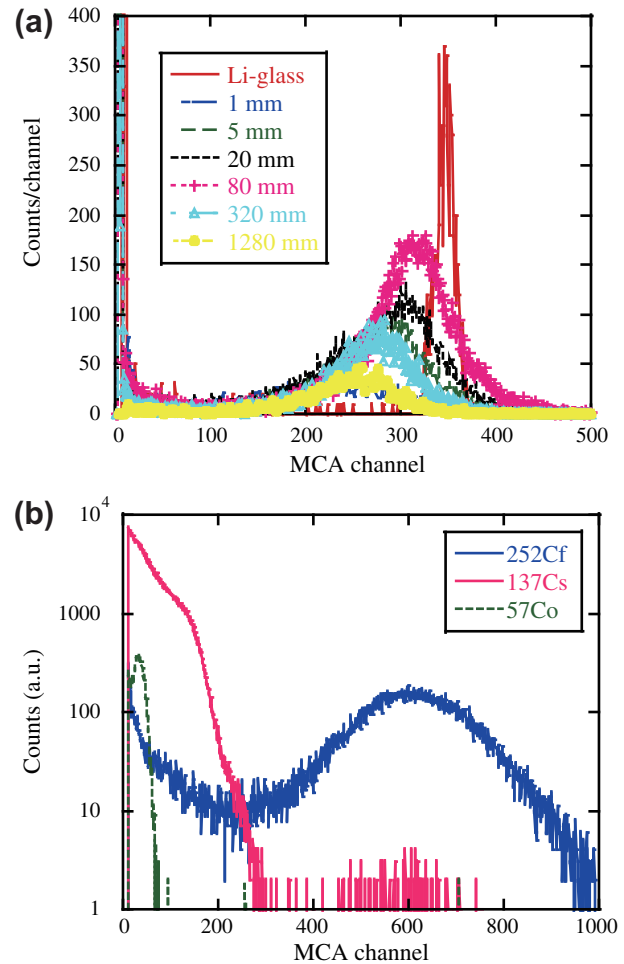


Fig. 5. (a) ²⁵²Cf neutron induced pulse height spectra of Ce 0.1% doped LiF-SrF₂ eutectics produced at different solidification rates (see inset), and (b) ¹³⁷Cs and ⁵⁷Co gamma-ray pulse height spectra and ²⁵²Cf neutron spectrum for the sample produced at 80 mm/hr.

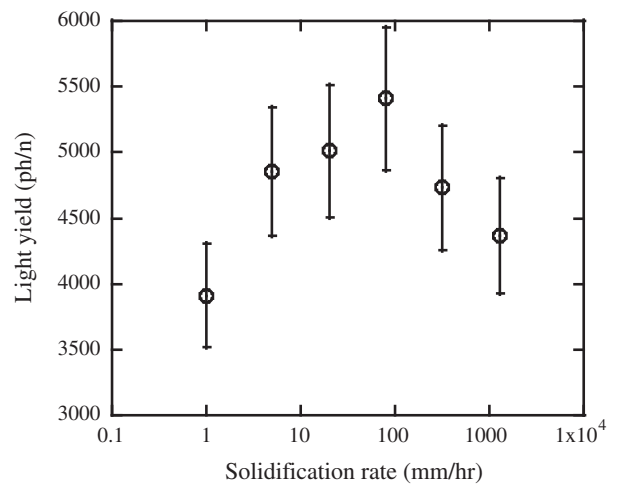


Fig. 6. Neutron induced scintillation light yield of Ce 0.1 % LiF-SrF₂ eutectics produced at different solidification rates.

slower component was 600–900 ns. The former one was similar to that of Ce doped SrF₂ [36], and its origin was attributed to Ce³⁺ 5d–4f emission. As compared with the previous results re-

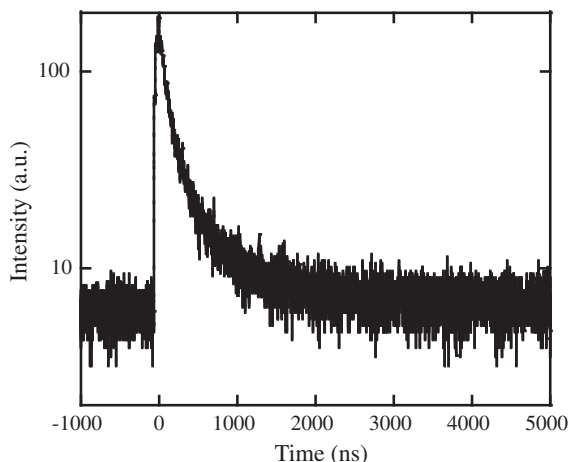


Fig. 7. Decay time profile of the sample produced at 80 mm/hr.

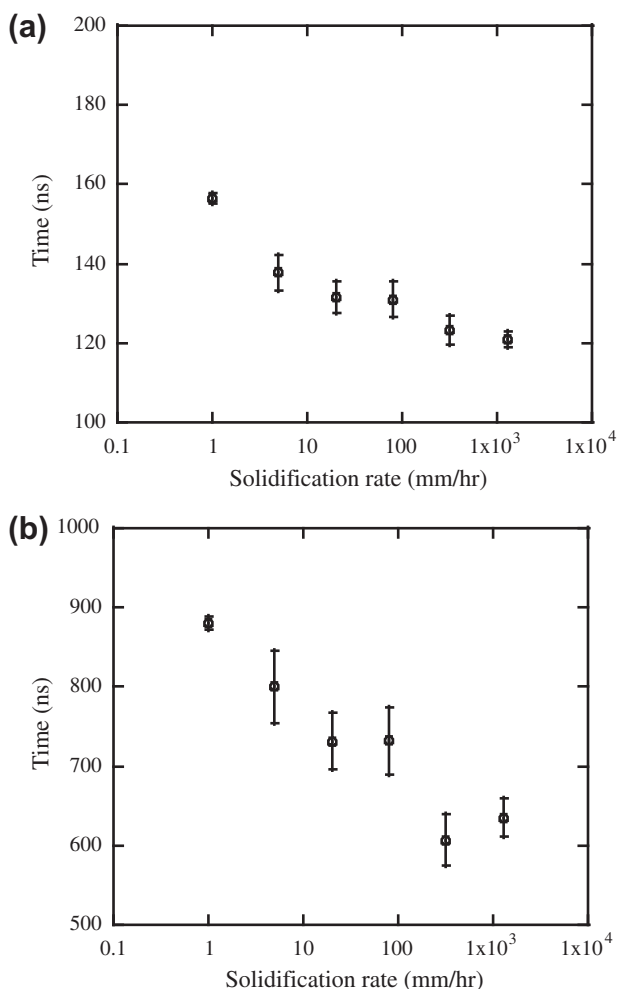


Fig. 8. Decay lifetimes of Ce^{3+} (a) and STE (b) emissions of Ce 0.1% doped LiF– SrF_2 eutectics vs. solidification rate.

ported in [37], the decay times observed here were slightly shorter (faster decay), and the difference is possibly result of presence of Cd^{2+} -additive (the main purpose was an oxygen scavenger) reported in [37]. The slower component was originated from the self-trapped exciton luminescence of SrF_2 itself because similar value (1 μs) was reported for pure SrF_2 [38]. The Ce^{3+} emission was faster when the solidification rate increased.

4. Conclusions

Ce^{3+} 0.1% activated LiF– SrF_2 eutectic scintillators were successfully grown by the vertical Bridgman method at various solidification rates to examine scintillation responses of these materials. It was confirmed that the LiF and SrF_2 layer thicknesses were dependant on the solidification rate. In ^{241}Am α -ray induced radioluminescence spectra, they demonstrated Ce^{3+} 5d–4f emission at 310 and 330 nm wavelengths. Among these samples, that produced at solidification rate of 80 mm/hr (layer thickness of 0.9 μm) had the highest light yield with a primary decay lifetime of 137 ns when characterized under ^{252}Cf neutron exposure.

Acknowledgments

This work was mainly supported by JST Sentan and partially by a Grant in Aid for Young Scientists (A)-23686135, and Challenging Exploratory Research-23656584 from the Ministry of Education, Culture, Sports, Science and Technology of the Japanese government (MEXT). Partial assistance from the Yazaki Memorial Foundation for Science and Technology, Shimazu Sci. Foundation, Kato Foundation for Promotion of Science, and Nippon Sheet Glass Foundation for Materials Science and Engineering is also gratefully acknowledged.

References

- [1] T. Yanagida, A. Yoshikawa, Y. Yokota, K. Kamada, Y. Usuki, S. Yamamoto, M. Miyake, M. Baba, K. Sasaki, M. Ito, IEEE Nucl. Trans. Sci. 57 (2010) 1492.
- [2] D. Totsuka, T. Yanagida, K. Fukuda, N. Kawaguchi, Y. Fujimoto, Y. Yokota, A. Yoshikawa, NIM Phys. Res. A 659 (2011) 399–402.
- [3] M. Kawaharada, S. Hong, M.M. Murashima, M. Kokubun, T. Itoh, K. Makishima, R. Miyawaki, H. Niko, T. Yanagida, T. Mitani, K. Nakazawa, K. Oonuki, T. Takahashi, K. Tamura, T. Tanaka, Y. Terada, Y. Fukazawa, N. Kawano, K. Kawashima, M. Ohno, K. Yamaoka, K. Abe, M. Suzuki, M. Tashiro, D. Yonetoku, T. Murakami, Proc. SPIE 5501 (2004) 286.
- [4] K. Yamaoka, M. Ohno, Y. Terada, S. Hong, J. Kotoku, Y. Okada, A. Tsutsui, Y. Endo, K. Abe, Y. Fukazawa, S. Hirakuri, T. Hiruta, K. Itoh, T. Itoh, T. Kamae, M. Kawaharada, N. Kawano, K. Kawashima, T. Kishishita, T. Kitaguchi, M. Kokubun, G.M. Madejski, K. Makishima, T. Mitani, R. Miyawaki, T. Murakami, M.M. Murashima, K. Nakazawa, H. Niko, M. Nomachi, K. Oonuki, G. Sato, M. Suzuki, H. Takahashi, I. Takahashi, T. Takahashi, S. Takeda, K. Tamura, T. Tanaka, M. Tashiro, S. Watanabe, T. Yanagida, D. Yonetoku, IEEE Trans. Nucl. Sci. 52 (2005) 2765.
- [5] C.L. Melcher, NIM Phys. Res. B 40 (41) (1989) 1214.
- [6] R.M. Brown, K. Deiters, Q. Ingram, D. Renker, NIM Phys. Res. A 695 (2012) 146.
- [7] I. Kanno, R. Imamura, Y. Minami, M. Ohtaka, M. Hashimoto, K. Ara, H. Onabe, NIM Phys. Res. A 695 (2012) 268.
- [8] R.C. Runkle, A. Bernstein, P.E. Vanier, J. Appl. Phys. 108 (2010) 111101.
- [9] R.T. Kouzes, The ^3He Supply Problem, Technical Rpt. PNNL-18388, Pacific Northwest National Laboratory, 2009.
- [10] R.T. Kouzes, J.H. Ely, A.T. Lintereur, E.K. Mace, D.L. Stephens, M.L. Woodring, NIM Phys. Res. A 654 (2011) 412.
- [11] T. Fujiwara, H. Takahashi, Y. Mitsuya, K. Kamada, T. Yanagida, K. Fukuda, N. Kawaguchi, Y. Fujimoto, M. Uesaka, IEEE NSS MIC 2011, Conference record, 2012, 1896–1897.
- [12] T. Yanagida, A. Yamaji, N. Kawaguchi, Y. Fujimoto, K. Fukuda, S. Kurosawa, A. Yamazaki, K. Watanabe, Y. Futami, Y. Yokota, A. Uritani, T. Iguchi, A. Yoshikawa, M. Nikl, Appl. Phys. Exp. 4 (2011) 106401.
- [13] T. Yanagida, A. Yoshikawa, Y. Yokota, S. Maeo, N. Kawaguchi, S. Ishizu, K. Fukuda, T. Suyama, Opt. Mater. 32 (2009) 311–314.
- [14] A. Yamazaki, K. Watanabe, A. Uritani, T. Iguchi, N. Kawaguchi, T. Yanagida, Y. Fujimoto, Y. Yokota, K. Kamada, K. Fukuda, T. Suyama, A. Yoshikawa, NIM Phys. Res. A 652 (2011) 435.
- [15] J. Iwanowska, L. Swiderski, M. Moszynski, T. Yanagida, Y. Yokota, A. Yoshikawa, K. Fukuda, N. Kawaguchi, S. Ishizu, NIM Phys. Res. A 652 (2011) 319.
- [16] T. Yanagida, N. Kawaguchi, Y. Fujimoto, K. Fukuda, Y. Yokota, A. Yamazaki, K. Watanabe, J. Pejchal, A. Uritani, T. Iguchi, A. Yoshikawa, Opt. Mater. 33 (2011) 1243–1247.
- [17] T. Yanagida, Opt. Mater., in press. 10.1016/j.optmat.2012.11.002.
- [18] T. Fujiwara, H. Takahashi, T. Yanagida, K. Kamada, K. Fukuda, N. Kawaguchi, N.L. Yamada, M. Furusaka, K. Watanabe, Y. Fujimoto, M. Uesaka, Neutron News 23 (2012) 31–34.
- [19] A. Chouiyakh, F. Gimeno, J.I. Pena, L. Contreras, V.M. Orera, Phys. Chem. News 13 (2003) 139.
- [20] J. Trojan-Piezza, J. Glodo, V.K. Sarin, Radiat. Meas. 45 (2010) 163.
- [21] N. Kawaguchi, K. Fukuda, T. Yanagida, Y. Fujimoto, Y. Yokota, T. Suyama, K. Watanabe, A. Yamazaki, A. Yoshikawa, NIM Phys. Res. A 652 (2011) 209.

- [22] T. Yanagida, K. Fukuda, Y. Fujimoto, N. Kawaguchi, S. Kurosawa, A. Yamazaki, K. Watanabe, Y. Futami, Y. Yokota, A. Yoshikawa, A. Uritani, T. Iguchi, *Opt. Mater.* 34 (2012) 868–871.
- [23] M. Campbell, K.W.D. Ledingham, A.D. Baillie, J.G. Lynch, *Nucl. Instrum. Meth.* 137 (1976) 235.
- [24] G.J. Davies, N.J.C. Spooner, J.D. Davies, G.J. Pyle, T.D. Bucknell, G.T.A. Squier, J.D. Lewin, P.F. Smith, *Phys. Lett. B* 322 (1994) 159–165.
- [25] D. Aliaga-Kelly, D.R. Nicoll, *NIM Phys. Res. A* 43 (1996) 110–115.
- [26] M.J. Weber, S.S. Derenzo, W. Moses, *J. Lumin.* 87–89 (2000) 830–832.
- [27] E. Loh, *Phys. Rev.* 147 (1966) 332–335.
- [28] T. Yanagida, K.J. Kim, K. Kamada, Y. Yokota, S. Maeo, A. Yoshikawa, N. Kawaguchi, K. Fukuda, N. Sarukura, V. Chani, *Jpn. J. Appl. Phys.* 49 (2010) 032601.
- [29] A.V. Gektin, N. Shiran, V. Nesterkina, Y. Boyarintseva, V. Baumer, G. Stryganyuk, K. Shimamura, E. Villora, *IEEE Trans. Nucl. Sci.* 56 (2009) 1002.
- [30] J.B. Czirr, E. Catalano, *NIM Phys. Res. A* 413 (1977) 487.
- [31] E. Renaud, C. Robelin, M. Heyrman, P. Chartrand, *J. Chem. Thermodynamics* 41 (2009) 666–682.
- [32] K. Mizukami, S. Sato, H. Sagehashi, S. Ohnuma, M. Ooi, H. Iwasa, F. Hiraga, T. Kamiyama, Y. Kiyana, *NIM Phys. Res. A* 529 (2004) 310–312.
- [33] H. Yang, N. Menea, F. Bronson, M. Kastner, R. Venkataraman, W.F. Mueller, *NIM Phys. Res. A* 652 (2011) 364.
- [34] H. Iikura, N. Tsutsui, T. Nakamura, M. Katagiri, M. Kureta, J. Kubo, M. Matsubayashi, *NIM Phys. Res. A* 651 (2011) 100.
- [35] T. Yanagida, K. Kamada, Y. Fujimoto, Y. Yokota, A. Yoshikawa, H. Yagi, T. Yanagitani, *NIM Phys. Res. A* 631 (2011) 54–57.
- [36] C.W.E. van Eijk, A. Bessiere, P. Dorenbos, *NIM Phys. Res. A* 529 (2004) 260.
- [37] R. Shendrik, E.A. Radzhabov, A.I. Nepomnyashchikh, [*cond-mat.mtrl-sci*], 2012.
- [38] R. Lindner, R.T. Williams, M. Reichling, *Phys. Rev. B* 63 (2001) 075110.